Liquid Crystals under Confinement in Submicrometer Capsules

Haiyan Peng,[†,⊥] Wenhong Jiang,[†,‡] Qingkun Liu,[§] Guannan Chen,[†] Mingli Ni,[†] Fuxin Liang,*[,‡] Yonggui Liao,[†,⊥] Xiaolin Xie,*[,†,⊥] and Ivan I. Smalyukh*[,⊥,§]

[†]Key Lab for Material Chemistry of Energy Conversion and Storage, Ministry of Education, and Hubei Key Lab of Material Chemistry and Service Failure, School of Chemistry and Chemical Engineering, Huazhong University of Science and Technology (HUST), Wuhan 430074, P. R. China

[‡]State Key Lab of Polymer Physics and Chemistry, Institute of Chemistry, Chinese Academy of Sciences, Beijing 100190, P. R. China

[§]Department of Physics and Materials Science and Engineering Program, University of Colorado at Boulder (CUB), Boulder, Colorado 80309, United States

[⊥]Sino−U.S. Joint Research Center on Liquid Crystal Chemistry and Physics, HUST and CUB

S *Supporting Information*

ABSTRACT: Liquid crystal (LC) ordering and phase transition behavior under confined conditions have attracted extensive attention and enabled many applications. However, the ordering and phase transition behavior of LCs in submicrometer capsules have seldom been studied, primarily due to the lack of proper capsulizing and visualization approaches to such small LC microcapsules. Herein, we achieve submicrometer LC capsules with the sizes down to 100 nm by using emulsion-based interfacial sol−gel reaction. The behavior of LCs under

the submicrometer confinement conditions is investigated while the sizes and chemical composition of the microcapsule shell surface are tuned in a controllable way. The phase transition temperatures of LCs in the submicrometer capsules shift from those of bulk LCs due to the surface-induced ordering of LCs under the strong confinement conditions, which causes formation of topological defects and alters the order parameter. Using nonlinear optical imaging technology, we explore the structures of director field of LCs that arise as a result of the competition between the surface boundary conditions and LC elasticity. The results show that the nanoscale encapsulation can significantly influence the structural configurations of the director and phase transitions of LCs under various confinement conditions.
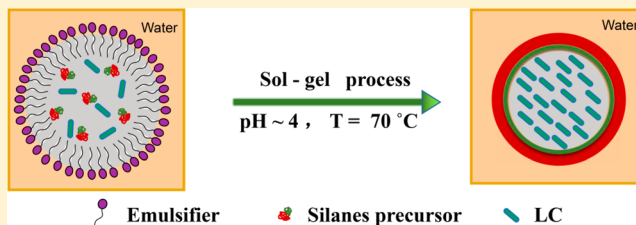
1. INTRODUCTION

Understanding the distinct behaviors of molecular assemblies under confined conditions at the nanoscale is not only of interest in fundamental science, but may also enable numerous practical applications. For instance, the confinement of ionic liquids by the inner surface of a multiwalled carbon nanotube dramatically increases the melting point of ionic liquids from 6 °C to more than 200 °C.[1] In comparison with ionic liquids, liquid crystals (LCs) are more sensitive to confined geometries because of the relatively weak internal interaction between LC mesogens. Consequently, LCs have unique capabilities of being readily responsive to external stimuli, such as surface alignment, electric fields above Freedericksz threshold, etc.[2] These external-force dependent molecular orientations allow for the selective light transmission by taking advantage of the large birefringence of LCs, which is the fundamental of LC display,[2,3] telepresence,[4] data storage,[5−8] laser modulating,[9] and other high-tech applications. Understanding the structural organization and phase transition behavior of LCs under confined conditions has been a long-term scientific pursue, and has enabled the design of new functional materials and devices for practical applications. In 1976, Sheng studied the nematic−isotropic phase transition of LCs in surface-aligned nematic films. By employing the Landau-de Gennes theory, he disclosed the critical thickness at which the phase transition was second order while below which the phase transition was continuous.[10] Miyano observed wall-induced birefringence in nematic LCs above the clearing temperature when the LCs were planarly aligned by an obliquely deposited SiO$_2$ film in a 1-μm thick cell.[11] Crawford and co-workers studied the phase transition of deuterated nematic LC 4-cyano-4′-pentylbiphenyl (5CB) confined in a 200 nm-wide cylindrical alumina channel. By employing magnetic resonance, they discovered a planar-to-homeotropic anchoring transition of LCs when increasing the chain length of the surface coupling agent on alumina.[12] Abbott, Caruso, and co-workers have investigated the confinement effect of LCs in a spherical geometry.[13−15] They observed bipolar, preradial, and radial ordering in multilayered polyelectrolyte-encapsulated 5CB droplets when the sizes of 5CB droplets decreased from 3 μm, 1 μm to 700 nm, respectively.[14]

Scheme 1. Illustrative Synthesis of (a) the Submicrometer LC Capsules by Emulsion Interfacial Sol-Gel Reaction, and (b) the Emulsifier HSMA
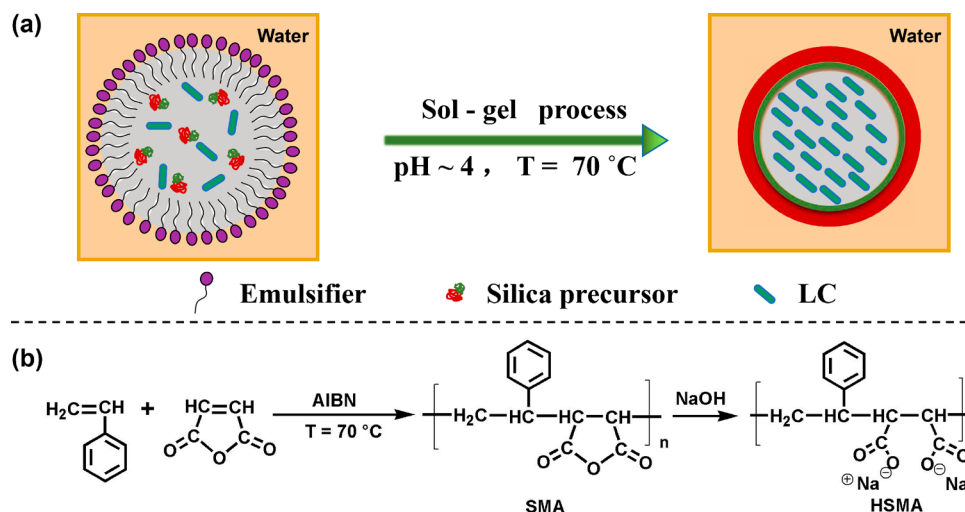
Such size-dependent LC ordering could be practically useful for detecting and distinguishing the species of surfactants, probing their concentrations in water,[14] and even detecting bacteria and viruses.[15] Zou and Fang demonstrated that such structural transformations depended on the polyelectrolyte used as well.[16] For instance, the poly(styrenesulfonic acid) coated 5CB droplets exhibited size-dependent bipolar-to-radial configuration transition, while the poly(styrenesulfonate sodium) coated 5CB had no such size effect. The bipolar ordering is caused by the tangential surface anchoring, while the radial configuration is typically related to homeotropic anchoring, though the interplay between surface anchoring and LC elasticity can be rather complex at the nanoscale. Deploying the tangential surface anchoring of LCs between two distinct layers in microspheres has successfully given rise to controlled photonic band gap for amplifying the upconversion luminescence.[17] Despite these substantial achievements, there remain numerous open questions and opportunities for furthering the fundamental understanding and applications of LCs in confined geometries. For instance, the submicrometer spherical capsules with the sizes smaller than 500 nm have not been studied so far, primarily due to the lack of proper capsulizing and visualization approaches to such nanoscale LC capsules. Although traditional layer-by-layer polyelectrolyte deposition,[18] microfluidic fabrication,[19] template-assisted processing,[13] and other methods have been employed to form spherical LC droplets, uniform submicrometer LC capsules less than 500 nm is rarely reported, to the best of our knowledge. Confinement of LCs into droplets with dimeter ~100 nm can cause interplay of surface anchoring energy with orientational elastic energy and reduction of order parameter through formation of defects that could have singular cores comparable to the droplet size, yielding very rich physical behavior different from that of bulk LC materials. The lack of LC capsules with narrowly dispersed sizes in submicrometer significantly hinders the fundamental understanding of the structural organization and phase transition behavior of LCs under such confinement.

Herein, we synthesized spherical LC capsules with diameters ranging from 800 nm down to 100 nm by emulsion interfacial sol−gel reaction (Scheme 1a). An emulsifier named hydrolyzed styrene-maleic anhydride (HSMA) copolymer (Scheme 1b) plays a critical role for the successful synthesis of these submicrometer LC capsules.[20] Traditional surfactants such as poly(vinyl alcohol) or sodium lauryl sulfate were found to be impractical to offer the similar submicrometer LC capsules. In addition, the chemical compositions of the capsule shell surface were easily tuned in a controllable way by employing different silane reactants. We studied structural configurations of director and phase transitions under various confinement conditions of different LCs, which is significantly influenced by the encapsulation. Furthermore, we used nonlinear optical imaging technique to explore the structures of director field, which arise as a result of the competition between the surface boundary conditions and LC elasticity. These novel nanoscale LC microcapsules are envisaged to play an important role for further understanding the confined ordering and phase transition behavior of LCs and show great promise for designing new functional materials and optical devices.

2. EXPERIMENTAL SECTION

2.1. Materials. LCs P0616A ($\Delta n_{(589\ nm,\ 20\ °C)}$ = 0.20, T_{NI} = 58 °C) and SLC123217−200 ($\Delta n_{(589\ nm,\ 20\ °C)}$ = 0.20, T_{NI} = 79 °C) were obtained from Shijiazhuang Chengzhi Yonghua Display Material Co., Ltd., China, both of which show nematic phase at room temperature. P0616A is a nonfluorinated cyanobiphenyl mixture, while SLC123217−200 is a fluorinated LC mixture. Phenyltriethoxysilane (PTES, purity 97%), n-octadecyltrimethoxysilane (ODTES, purity 90%), n-octyltriethoxysilane (OTES, purity 97%), 3-methacryloxypropyltrimethoxysilane (MPS, purity 97%), and γ-aminopropyltriethoxysilane (APTES, purity 98%) were purchased from Alfa Aesar. Tetraethyl orthosilicate (TEOS, AR) was purchased from Sinopharm Chemical Reagent Beijing Co., China. Styrene (distilled), maleic anhydride and 2,2-azobis(2-methylpropionitrile) (AIBN) (recrystallized from methanol prior to use) were purchased from Aldrich. The styrene-maleic anhydride (SMA) copolymer was synthesized via free radical polymerization. All reagents were used as-received without further purification if not specified.

2.2. Synthesis of HSMA. A copolymerization of styrene and maleic anhydride at a 1:1 molar ratio was carried out by a precipitation polymerization method. In a 250 mL three-neck round-bottom flask, 150 mL of toluene, 5.8 mL of styrene (0.051 mol), 5.0 g of maleic anhydride (0.051 mol), and 0.01 g of AIBN were added under stirring. After being purged with nitrogen gas for 30 min, the mixture was heated to 85 °C and refluxed for 2 h. The resulting copolymer SMA (styrene-maleic anhydrite) was separated by filtration, and washed with toluene to remove residual reactants. The product was
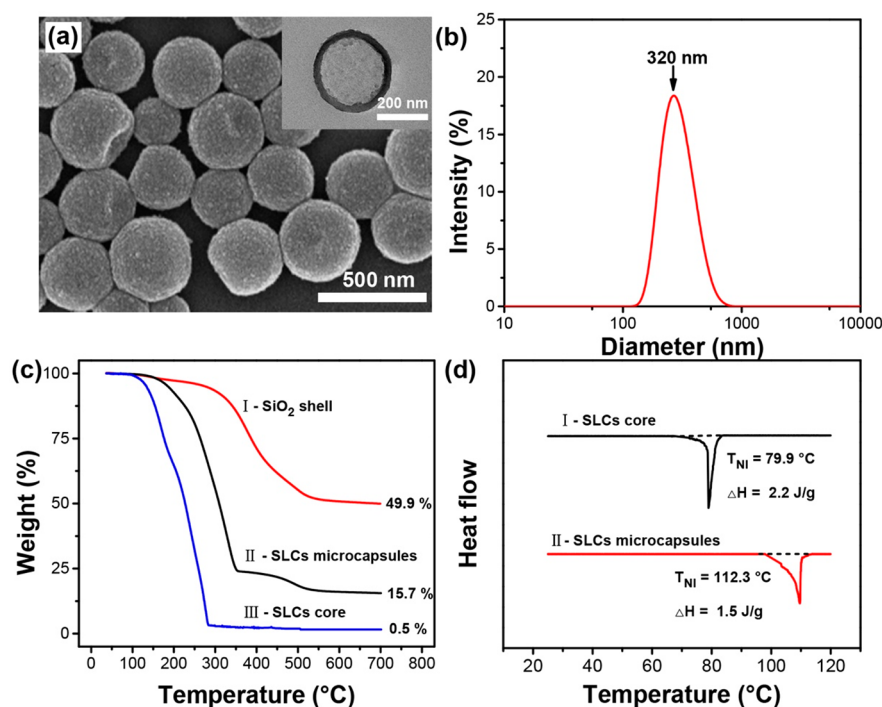
Figure 1. (a) SEM image (inset: TEM image) of the SLCs microcapsules with a diameter of 325 ± 37 nm; (b) DLS result of the SLCs microcapsules dispersed in water giving a diameter of 320 nm with a polydispersity index (PDI) of 0.07; (c) TGA curves of the organic-molecule functionalized SiO_2 shell of microcapsules after removing SLCs (I), SLCs microcapsules (II), and pristine SLCs without capsulation (III), respectively; (d) DSC curves of the pristine SLCs (I) and SLCs microcapsules (II), separately. The dashed lines were employed as the baselines for calculating the phase transition enthalpy. The SLCs core indicates the pristine bulk SLCs prior to encapsulation.
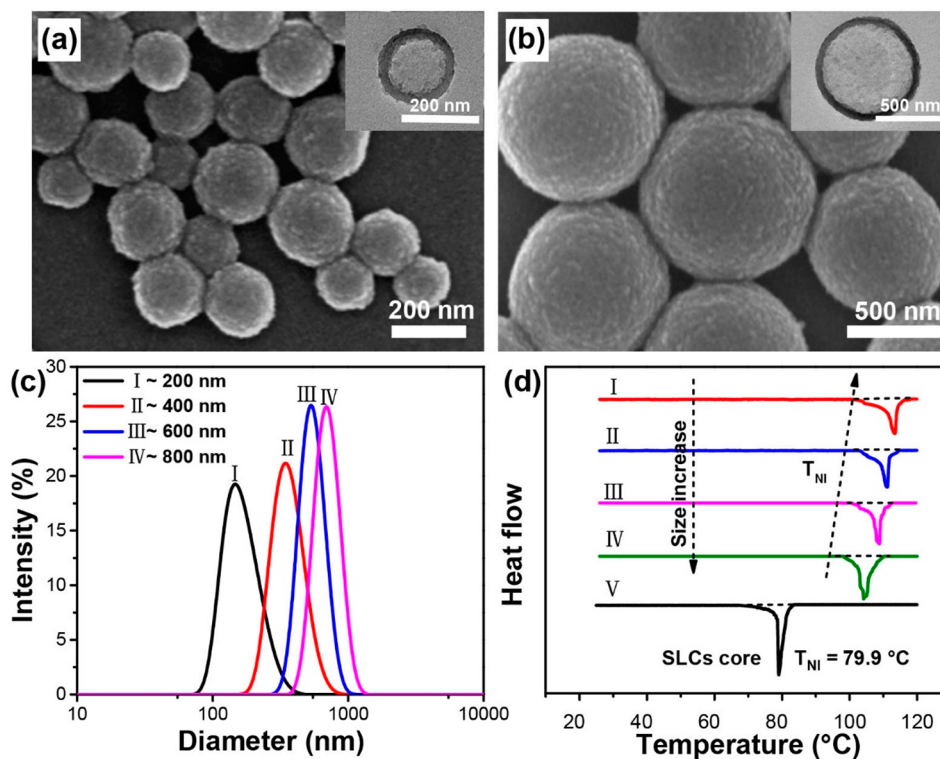

Figure 2. (a, b) SEM images (inset: TEM images) of the SLCs microcapsules with varied diameters: (a) 213 ± 30 nm, (b) 833 ± 66 nm, respectively; (c) DLS and (d) DSC results of the SLCs microcapsules with different diameters, (I) 200 nm with a PDI of 0.08, T_{NI} = 113.4 °C, ΔH = 1.3 J/g; (II) 400 nm with a PDI of 0.05, T_{NI} = 111.1 °C, ΔH = 1.6 J/g; (III) 600 nm with a PDI of 0.15, T_{NI} = 108.7 °C, ΔH = 1.8 J/g; (IV) 800 nm with a PDI of 0.29, T_{NI} = 102.9 °C, ΔH = 2.0 J/g; (V) SLCs, T_{NI} = 79.9 °C, ΔH = 2.2 J/g. The dashed lines were employed as the baselines to calculate the phase transition enthalpy.

Scheme 2. Chemical Structures of the Hydrophobic Functional Groups on the Microcapsule Shell Surface[a]
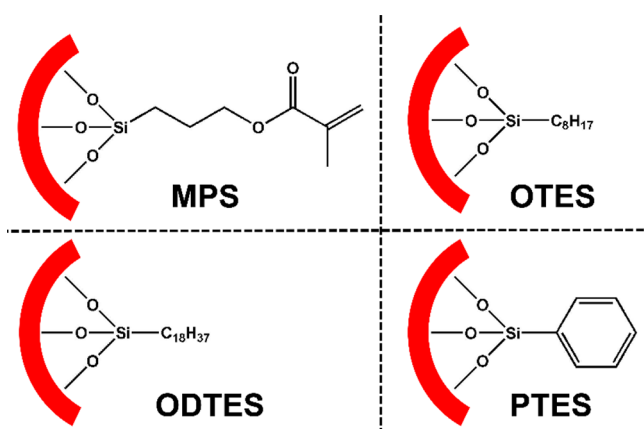
[a]Methacryloxypropyl, octadecyl, octyl and phenyl groups were chemically attached on the SiO_2 shell, respectively, by using the precursors of MPS, OTES, ODTES, and PTES.

Figure 3. SEM images (inset: TEM images) for the microcapsules with different organic functional groups on the microcapsule shell surface: (a) methacryloxypropyl, (b) octyl, (c) octadecyl, and (d) phenyl group, respectively. The capsule size was determined from SEM to be 400 ± 24, 416 ± 40, 404 ± 40, and 414 ± 50 nm, respectively.

finally dried in an oven at 60 °C under reduced pressure. The anionic emulsifier, HSMA, was obtained through hydrolysis of the SMA copolymer. The SMA powder (10.0 g) was dissolved in 90 g of 3 wt % sodium hydroxide solution under stirring at 80 °C for 3 h, giving rise to a transparent solution with approximate 10 wt % of HSMA.

2.3. Synthesis of Submicrometer LC Capsules. A representative recipe of synthesizing submicrometer LC capsules is described as follows. A 10 mL aqueous solution with 10 wt % of HSMA was diluted by another 80 mL of water to form the aqueous phase. The solution pH was adjusted to ~4 with 2 M aqueous hydrochloric acid. 0.85 g of APTES, 0.80 g of MPS, and 3.35 g of TEOS were dissolved in 5 g of LCs as the oil phase. The total gross mass of silanes and LCs was fixed at 10 g. Then the oil phase and aqueous phase were mixed together and emulsified under shearing using a high-speed disperser, offering an oil-in-water emulsion. The emulsion was held under stirring at 300 rpm at 70 °C for 7 h to allow for complete reaction. When the resultant emulsion was cooled down to ambient temperature, the core/shell spheres were obtained by washing with water for 3 times and then freeze-dried. The size of as-formed microspheres was tuned from 100 to 800 nm via varying the stirring speed and duration during emulsifying. Moreover, the surface functionalization of the shell of LC microcapsules could be tuned by changing the silica precursors with specific organic groups.

2.4. Characterization. The morphology of the LC microcapsules was characterized using transmission electron microscopy (TEM, JEOL 100CX operated at 100 kV) and scanning electron microscopy (SEM, S-4800 at 15 kV). The samples for SEM observation were sputtered with platinum on the top surface. Prior to TEM characterization, ethanol was employed to remove the internal LCs inside the microcapsules to enhance the image contrast. Then, dilute dispersions of the hollow SiO_2 shells in ethanol were spread onto carbon-coated copper grids and dried at room temperature. The size distribution of LC microcapsules in an aqueous dispersion was measured by dynamic light scattering (DLS) in Zetasizer (Nano Series, Malvern Instruments). The LC content in each microcapsule was determined under air by heating the sample to 700 °C at a ramp rate of 10 °C/min using thermogravimetric analysis (TGA Pyris1, PerkinElmer). The phase transition behavior was characterized in a temperature range from 25 to 120 °C under nitrogen atmosphere at a heating rate of 5 °C/min in a differential scanning calorimeter (DSC, Q2000, TA Instruments, U.S.A.). The samples have been heated to 120 °C (above the nematic–isotropic transition temperatures of the used LCs) to eliminate the thermal effect on LC director fields before characterizing them.

The structure of the LC director field inside microcapsules was visualized and then reconstructed using a home-built three-photon excitation fluorescence polarizing microscope (3PEF-PM) based on
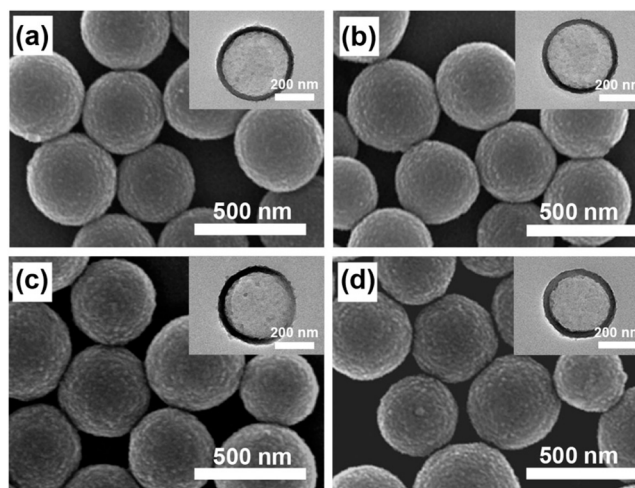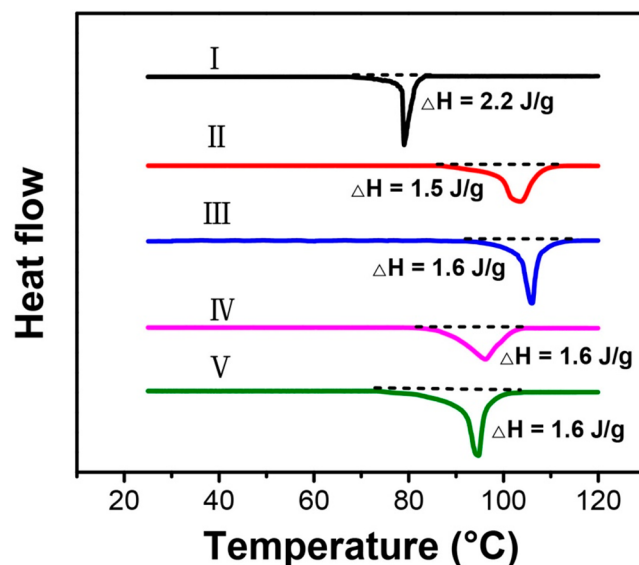

Figure 4. DSC curves of the SLCs microcapsules with different functional groups on the shell surface. (I) Pristine SLCs, T_{NI} = 79.9 °C; (II) methacryloxypropyl functionalized SLCs microcapsules, T_{NI} = 103.5 °C; (III) octyl functionalized SLCs microcapsules, T_{NI} = 105.9 °C; (IV) octadecyl functionalized SLCs microcapsules, T_{NI} = 96.1 °C; (V) phenyl functionalized SLCs microcapsules, and T_{NI} = 94.7 °C. The dashed lines were employed as the baselines for calculating the phase transition enthalpy.

an inverted optical microscope IX-81 (Olympus). The polarization-dependent fluorescence from LC molecules was excited via a three-photon absorption process by a Ti:sapphire laser (Chameleon Ultra II, Coherent). The excitation source laser operated at 870 nm, with 140 fs pulses and repetition frequency of 80 MHz. The 400–500 nm 3PEF-PM signal of LCs was collected by a photomultiplier tube (H5784-20, Hamamatsu) and an oil-immersion 100× objective (numerical aperture NA = 1.4). The 3PEF-PM technique allows for the reconstruction of three-dimensional director structures on the basis of stacks of two-dimensional scans of LC samples obtained at different polarizations of excitation light, as detailed below. The 3PEF-PM technique principles and its implementation are described in details elsewhere.[21,22]
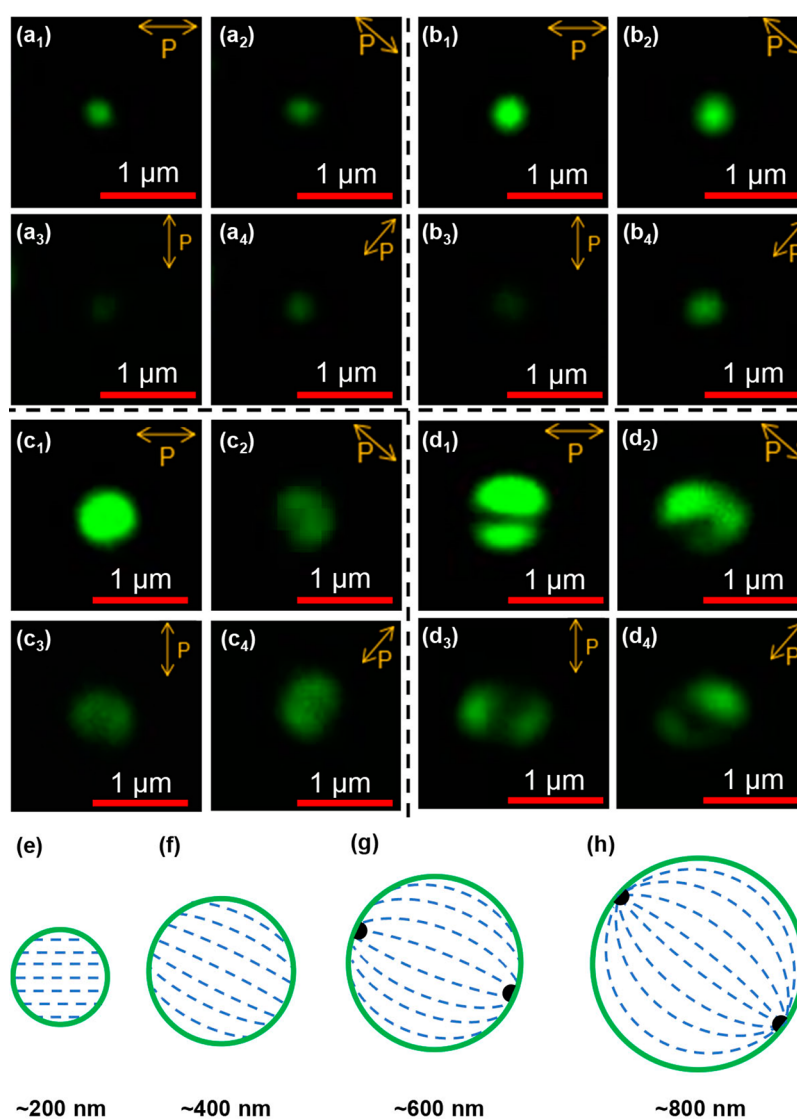
Figure 5. Three-photon excitation fluorescence polarizing microscopy images of director field for the SLCs microcapsules with varied diameter: (a) ~200 nm, (b) ~400 nm, (c) ~600 nm, and (d) ~800 nm, respectively. (e−h) The configurations of SLCs director in the size-controlled microcapsules, where these configurations were reconstructed from the three-photon excitation polarized fluorescence images shown in (a−d), respectively. The points of discontinuity of the director field (dashed lines) in (g, h) indicate the two surface defects called "boojums".

3. RESULTS AND DISCUSSION

3.1. Capsulizing LCs without Composition Change. Submicrometer LC capsules were formed through the sol−gel reaction at the emulsion oil−water interface, as illustrated in Scheme 1a. Silanes of TEOS and APTES were typically together employed to form the SiO$_2$ shells. TEOS worked as a cross-linking agent while APTES provided hydrophilic aminopropyl groups on the shell surface. After being stirred at 70 °C for 7 h, LC microcapsules with rigid SiO$_2$ shells and soft LC cores were formed. With careful variation of the silanes/LCs mass ratio, emulsion pH, shear speed and duration prior to the sol−gel reaction, spherical LC microcapsules with narrowly distributed sizes and smooth surface were readily achieved, and their diameters were able to be controlled from 100 to 800 nm, separately (Figures S1−S4 in the Supporting Information, SI). Initially, fluorinated LCs SLC123217−200 (namely SLCs), were encapsulated to achieve LC microcapsules. Spherical SLCs microcapsules with an average diameter of ~320 nm and a shell thickness of ~30 nm were first prepared (Figure 1a, b).

The low polydispersity index (PDI) of 0.07 from DLS characterization indicates the narrow distribution of the microcapsule size. TGA results show that the residue at 700 °C after heat treatment under air is 49.9%, 15.7%, and 0.5 wt % for the rigid SiO$_2$ shell, SLCs microcapsules, and pristine SLCs core, respectively (Figure 1c), indicating a LC content of ~68 wt % in the LC microcapsules. The LC content was determined using the following formula, (1-residue mass of LC microcapsules/ residue mass of SiO$_2$ shell) × 100%. DSC analysis shows that the phase transition temperature of SLCs in the microcapsules increases 32.4 °C (i.e., from 79.9 °C to 112.3 °C) in compassion to the pristine bulk SLCs due to the large confinement (Figure 1d).

A temperature shift for phase transition is a result of different competing effects. In general, surface induced ordering gives rise to an increased phase transition temperature, while the elastic force induced disordering reduces the phase transition temperature.[23] We speculate that the SLC molecules are tangentially aligned by the inner surface of microcapsules. It is reasonable that a tangential alignment of LC molecules inside
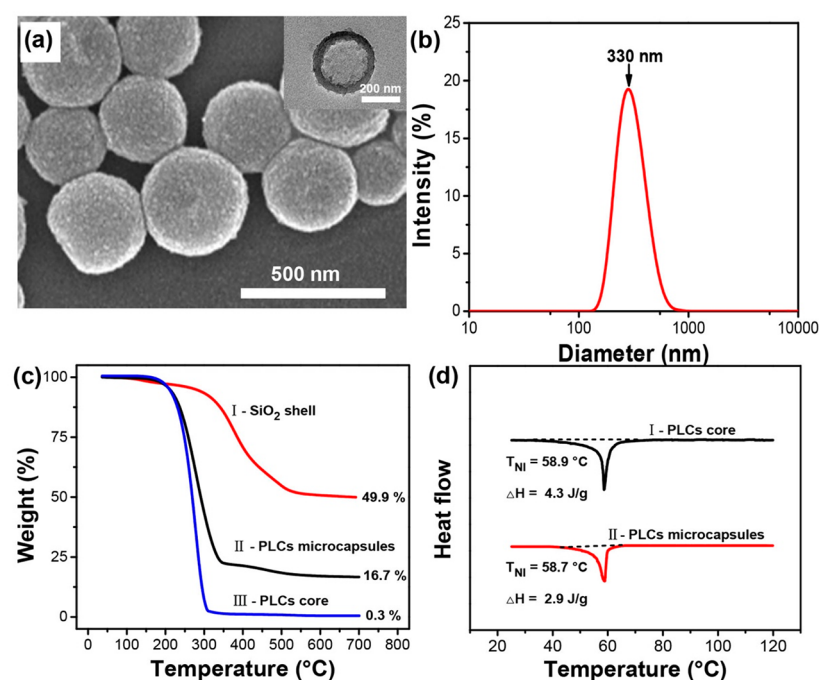
Figure 6. (a) SEM image (inset: TEM image) of the PLCs microcapsules with a diameter of 328 ± 28 nm; (b) DLS of the PLCs microcapsules dispersed in water indicating a diameter of 330 nm with a PDI of 0.08; (c) TGA of the SiO₂ shell of microcapsules after removing PLCs (I), PLCs microcapsules (II), and pristine PLCs (III), respectively; (d) DSC curves of the pristine PLCs (I) and PLCs microcapsules (II), separately. The dashed lines were used as baselines to calculate the phase transition enthalpy. The PLCs core indicates the pristine bulk PLCs prior to encapsulation.

the microcapsule is able to increase the nematic ordering[11] and thus to increase the phase transition temperature. We can further predict that a stronger confinement would be generated in a smaller LC microcapsule, which requires more thermal energy to overcome the aligning action of surface anchoring and to allow for the nematic−isotropic phase transition,[24] which will be discussed in the following section. Notably, the apparent enthalpy per gram sample decreases by 31.8% due to the decreased LC content inside the smaller LC microcapsules. However, the phase transition enthalpy per gram SLCs remains (i.e., 2.2 J/g) by taking the LC content (∼68 wt %) into consideration. The unchanged intrinsic phase transition enthalpy implies that there is no significant LC molecular loss or impurity introduced into the SLCs core during the microcapsule preparation. We note that the intrinsic enthalpy can change if the compositions of LC mixtures vary or a small amount of impurities are introduced.[25]

3.2. Size Effect of the LC Microcapsules on Fluorinated LCs.

To further understand the size effect on the confinement, spherical LC microcapsules with diameters from 100 to 800 nm were prepared by varying the shear rate and the duration of emulsification. When fixing the shear rate at 13000 rpm while increasing the shear duration from 4 to 5 min, the average diameter of SLCs microcapsules decreased from ∼320 to ∼200 nm (Figure 1a and 2a). On the contrary, the diameter of the SLCs microcapsules increased to 800 nm in response to decreasing the shear rate and duration to 10 000 rpm and 3 min, simultaneously (Figure 2b, c). DSC analysis clearly depicts that the phase transition temperature continuously increases from 79.9 °C to 111.1 °C for the pristine SLCs, when the microcapsule diameter reduces to 400 nm from 800 nm (Figure 2d). Further decrease of the SLCs microcapsule size to 200 nm leads to a slight augmentation of the phase transition

temperature by 2.3 °C. A smaller microcapsule is envisioned to afford larger confinement on the SLCs molecules by the capsule shell.[23] The nematic−isotropic phase transition enthalpy (i.e., 2.2 J/g) does not change for per gram SLCs with varied microcapsule sizes, considering the varied SLCs content in each microcapsule (Figure S5 in the SI), indicating that the confinement energy at the microcapsule shell/LC interface has negligible effect on the phase transition enthalpy in the bulk LCs. As aforementioned, smaller microcapsules afford much larger confinement on the SLCs and consequently higher phase transition temperatures. For instance, no phase transition peak is detectable in DSC for the LC microcapsules with a diameter of 100 nm because of the very strong surface confinement (Figure S4 in the SI).

3.3. Functional Group Effect of LC Microcapsules on Fluorinated LCs.

To get a deeper insight into the interface interaction, we synthesized other four SLCs microcapsules with varied chydrophobic organic functional groups on the shell surface, e.g., methacryloxypropyl, octyl, octadecyl, and phenyl groups, respectively (Scheme 2). The functionalization was readily implemented by selecting specific silane reagents. To avoid the size influence, LC microcapsules with an average diameter of ∼400 nm and shell thickness of ∼35 nm were prepared (Figure 3). DSC analysis reveals that the phase transition temperature of the as-encapsulated SLCs is 103.5 °C, 105.9 °C, 96.1 °C, and 94.7 °C, respectively, when the shell surfaces are coated with methacryloxypropyl, octyl, octadecyl, and phenyl groups, individually (Figure 4). It is clear that the SLCs microcapsules with more hydrophobic groups on the shell surface exhibit lower phase transition temperature than those with more hydrophilic groups (i.e., 111 °C, Figure 2d). More hydrophilic groups on the microcapsule shell surface are believed to offer larger van der Waals interaction with the electrophilic
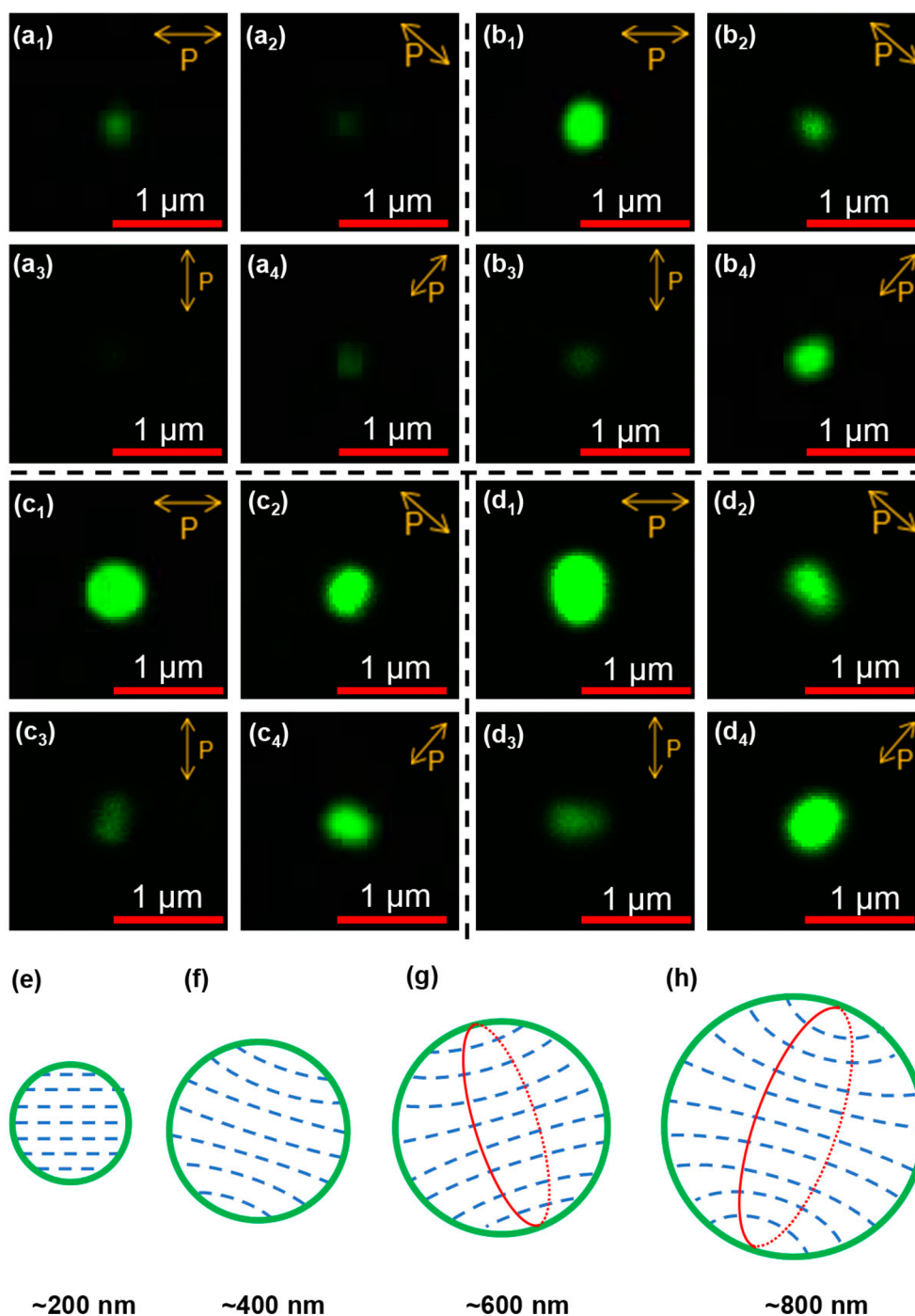
Figure 7. Three-photon excitation fluorescence polarizing microscopy images for the PLC microcapsules with varied diameters: (a) ~200 nm, (b) ~400 nm, (c) ~600 nm, and (d) ~800 nm, respectively. (e−h) The configurations of PLCs director in microcapsules reconstructed from the 3PEF−PM images shown in (a−d), respectively. The director field is shown in dashed lines.

SLC molecules because of the high electronegativity of the fluorine atom,[26,27] which leads to higher interfacial anchoring energy on the SLCs and consequently higher phase transition temperatures. Nevertheless, the phase transition enthalpy does not change for per gram SLCs microcapsules, and per gram SLCs, regardless of the functional groups on the shell surface.

3.4. Structural Configurations of Fluorinated LCs in Microcapsules. We further investigated the director configurations in the LC microcapsules using the 3PEF-PM imaging. This imaging technique is based on the self-fluorescence of

LC molecule without any added dye. The high polarization dependence of the 3PEF-PM fluorescence allows for the reconstruction of complex 3D director fields of LCs in the microcapsules. The 3PEF-PM intensity scales as $\propto \cos^6 \psi_{3PEF}$, where ψ_{3PEF} is the angle between the director $\mathbf{n}(\mathbf{r})$ and the linear polarization of the excitation laser light.[28−30] Microcapsules with aminopropyl functionalized shells were employed for this investigation. As we show in Figure 5a−d, 200 nm (the smallest) microcapsules exhibit uniform polarized fluorescence patterns while the largest droplets show spatially varying polarized fluorescence patterns. On the basis of polarization dependence of

these fluorescence features, we reconstruct the size-dependent director structures (Figure 5e–h).

Because of the tangential alignment of SLCs molecules along the inner SiO_2 shell surface, the director configuration depends on the competition between the surface anchoring energy and the bulk elasticity of SLCs. Taking account of the bulk elastic energy scaling as $F_e \approx KR$ and the surface anchoring energy scaling as $F_s \approx WR$,[2] the director of SLCs relies on the radius of LC droplet confined inside the SiO_2 shell, R, where K is the elastic constant, and W is the polar surface anchoring coefficient, when R is smaller than the correlation length $\xi = K/W$, which is in the range of several hundred nanometers, uniform alignment of the director for SLCs appears. With increasing the radius of silica shell, the director of SLCs changes from the uniform alignment into bipolar configuration, consistent with our experimental observations (Figure 5). The configuration change from bipolar into uniform alignment when decreasing the microcapsule size results in much higher surface anchoring energy, which consequently gives rise to increased phase transition temperatures, as described in Figure 2.

3.5. Size Effect of the LC Microcapsules on Non-fluorinated LCs. We also studied nonfluorinated LCs, such as the commercially available system P0616A.[31] After being stirred at 70 °C for 7 h, the as-used silanes of TEOS and APTES reacted at the oil–water interface of emulsion via sol–gel process, giving rise to rigid inorganic SiO_2 shells that encapsulated P0616A as the core. Such nonfluorinated LC microcapsules were referred to as PLCs microcapsules. The first as-synthesized PLCs microcapsules are spherical and in ~330 nm as well, with a shell thickness of ~32 nm (Figure 6a, b), consistent with the morphology of the SLCs microcapsules shown in Figure 1a. The LC content in these microcapsules is calculated to be ~67 wt % according to the TGA characterization (Figure 6c). What is interesting is that neither variation of the phase transition temperature nor change of the phase transition enthalpy per gram LCs is observed in these PLCs microcapsules according to the DSC characterization (Figure 6d), quite distinct from that observed in the SLCs microcapsules (Figure 1d). We speculate that the PLC molecules are homeotropically aligned on the shell/LC interface. Such alignment is expected to generate disclination line defects that give rise to reduced phase transition temperature. Iannacchione and Finotello obeserved a temperature decrease of 1.1 °C for the phase transition in a radial configuration because of the homeotropic alignment, compared to the bulk LC.[32] However, the temperature decrease might be too small to be detected using DSC if the microcapsule size is over 100 nm.[23] Under such condition, no phase transition temperature change can be detected either varying the microcapsule size or changing the interfacial property (Figures S6–S8 in the SI). The lack of the significant effect of confinement on the LC behavior in this case might be related to the potentially weak strength of surface boundary conditions, although a detailed theoretical exploration of this effect would require Q-tensor based modeling and is beyond the scope of the present study. However, the configuration change from homeotropic alignment to uniform alignment under these confinement conditions is confirmed using the three-photon excitation fluorescence polarizing microscopy (Figure 7).

When the radius of LC droplet is smaller than the correlation length ξ, the LC director shows rather uniform alignment. By contrast, when the radius of LC droplet increases, the PLCs director changes from the uniform alignment into a configuration with a ring of half-integer disclination line. The reconstructed director configurations are depicted in Figure 7e–h. By comparing results for SLCs and PLCs microcapsules, we conclude that the former exhibit tangential surface boundary conditions for the LC, and thus give rise to a positive shift of the phase transition temperature. The mechanism why fluorinated and nonfluorinated LCs exhibit different boundary conditions is still under study. Since the fluorine atom holds a larger electronegativity value in comparison with the hydrogen atom, the fluorinated LCs with several fluorine atoms possibly show larger interaction with oxygen and nitrogen on the capsule surface, consequently giving rise to a tangential alignment. In both cases, the size-dependent behavior of director structures is consistent with what one can expect on the basis of competing surface anchoring and bulk elasticity effects.

4. CONCLUSIONS

In summary, we synthesized spherical submicrometer LC microcapsules with diameters ranging from 100 to 800 nm using the emulsion interfacial sol–gel reaction for the first time. The configurations of the LC director field were carefully analyzed using the three-photon excitation fluorescence polarizing microscopy, revealing that the director configuration arises from balancing the surface anchoring and bulk elasticity effects. For the fluorinated LCs, a change from bipolar configuration into uniform alignment was observed when decreasing the microcapsule size, because of the tangential molecular alignment of LC on the interface. For this confinement, a significant increase of the phase transition temperature was observed. In contrast, a change of homeotropic-polar configuration into uniform alignment was revealed for the nonfluorinated LCs, while phase transition temperature remained practically unchanged. This study paves a way for transformation study in confinement conditions and the arrangement of LCs.

■ ASSOCIATED CONTENT

ⓢ Supporting Information

The Supporting Information is available free of charge on the ACS Publications website at DOI: 10.1021/acs.langmuir.8b01056.

> Optimization of conditions for preparing submicrometer LC capsules, LC content determination on the basis of TGA, and characterization of nonfluorinated LC microcapsules, Figures S1–S8 (PDF)

■ AUTHOR INFORMATION

Corresponding Authors
*E-mail: liangfuxin@iccas.ac.cn (F. L.).
*E-mail: xlxie@mail.hust.edu.cn (X. X.).
*E-mail: Ivan.Smalyukh@colorado.edu (I. S.).
ORCID Ⓞ
Haiyan Peng: 0000-0002-0083-8589
Yonggui Liao: 0000-0003-2943-1501
Xiaolin Xie: 0000-0001-5097-7416
Ivan I. Smalyukh: 0000-0003-3444-1966
Notes
The authors declare no competing financial interest.

■ ACKNOWLEDGMENTS

■ REFERENCES

(1) Chen, S.; Wu, G.; Sha, M.; Huang, S. Transition of ionic liquid [BMIM][PF₆] from liquid to high-melting-point crystal when confined in multiwalled carbon nanotubes. *J. Am. Chem. Soc.* **2007**, *129* (9), 2416−2417.

(2) Geelhaar, T.; Griesar, K.; Reckmann, B. 125 Years of liquid crystals-A scientific revolution in the home. *Angew. Chem., Int. Ed.* **2013**, *52* (34), 8798−8809.

(3) Fattal, D.; Peng, Z.; Tran, T.; Vo, S.; Fiorentino, M.; Brug, J.; Beausoleil, R. G. A multi-directional backlight for a wide-angle, glasses-free three-dimensional display. *Nature* **2013**, *495* (7441), 348−351.

(4) Blanche, P. A.; Bablumian, A.; Voorakaranam, R.; Christenson, C.; Lin, W.; Gu, T.; Flores, D.; Wang, P.; Hsieh, W. Y.; Kathaperumal, M.; Rachwal, B.; Siddiqui, O.; Thomas, J.; Norwood, R. A.; Yamamoto, M.; Peyghambarian, N. Holographic three-dimensional telepresence using large-area photorefractive polymer. *Nature* **2010**, *468* (7320), 80−83.

(5) Bruder, F. K.; Hagen, R.; Rolle, T.; Weiser, M. S.; Facke, T. From the surface to volume: Concepts for the next generation of optical-holographic data-storage materials. *Angew. Chem., Int. Ed.* **2011**, *50* (20), 4552−4573.

(6) Peng, H. Y.; Bi, S. G.; Ni, M. L.; Xie, X. L.; Liao, Y. G.; Zhou, X. P.; Xue, Z. G.; Zhu, J. T.; Wei, Y.; Bowman, C. N.; Mai, Y. W. Monochromatic visible light "photoinitibitor": Janus-faced initiation and inhibition for storage of colored 3D images. *J. Am. Chem. Soc.* **2014**, *136* (25), 8855−8858.

(7) Chen, G. N.; Ni, M. L.; Peng, H. Y.; Huang, F. H.; Liao, Y. G.; Wang, M. K.; Zhu, J. T.; Roy, V. A. L.; Xie, X. L. Photoinitiation and inhibition under monochromatic green light for storage of colored 3D images in holographic polymer-dispersed liquid crystals. *ACS Appl. Mater. Interfaces* **2017**, *9* (2), 1810−1819.

(8) Ni, M. L.; Peng, H. Y.; Xie, X. L. Structure regulation and performance of holographic polymer dispersed liquid crystals. *Acta Polym. Sin.* **2017**, *48* (10), 1557−1573.

(9) Stolyarov, A. M.; Wei, L.; Shapira, O.; Sorin, F.; Chua, S. L.; Joannopoulos, J. D.; Fink, Y. Microfluidic directional emission control of an azimuthally polarized radial fibre laser. *Nat. Photonics* **2012**, *6* (4), 229−233.

(10) Sheng, P. Phase transition in surface-aligned nematic films. *Phys. Rev. Lett.* **1976**, *37* (16), 1059−1062.

(11) Miyano, K. Wall-induced pretransitional birefringence: A new tool to study boundary aligning forces in liquid crystals. *Phys. Rev. Lett.* **1979**, *43* (1), 51−54.

(12) Crawford, G. P.; Ondriscrawford, R.; Zumer, S.; Doane, J. W. Anchoring and orientational wetting transitions of confined liquid crystals. *Phys. Rev. Lett.* **1993**, *70* (12), 1838−1841.

(13) Sivakumar, S.; Gupta, J. K.; Abbott, N. L.; Caruso, F. Monodisperse emulsions through templating polyelectrolyte multilayer capsules. *Chem. Mater.* **2008**, *20* (6), 2063−2065.

(14) Gupta, J. K.; Sivakumar, S.; Caruso, F.; Abbott, N. L. Size-dependent ordering of liquid crystals observed in polymeric capsules with micrometer and smaller diameters. *Angew. Chem., Int. Ed.* **2009**, *48* (9), 1652−1655.

(15) Sivakumar, S.; Wark, K. L.; Gupta, J. K.; Abbott, N. L.; Caruso, F. Liquid crystal emulsions as the basis of biological sensors for the optical detection of bacteria and viruses. *Adv. Funct. Mater.* **2009**, *19* (14), 2260−2265.

(16) Zou, J.; Fang, J. Director configuration of liquid-crystal droplets encapsulated by polyelectrolytes. *Langmuir* **2010**, *26* (10), 7025−7028.

(17) Kang, J. H.; Kim, S. H.; Fernandez-Nieves, A.; Reichmanis, E. Amplified photon upconversion by photonic shell of cholesteric liquid crystals. *J. Am. Chem. Soc.* **2017**, *139* (16), 5708−5711.

(18) Driever, C. D.; Mulet, X.; Johnston, A. P. R.; Waddington, L. J.; Thissen, H.; Caruso, F.; Drummond, C. J. Converging layer-by-layer polyelectrolyte microcapsule and cubic lyotropic liquid crystalline nanoparticle approaches for molecular encapsulation. *Soft Matter* **2011**, *7* (9), 4257−4266.

(19) Lee, T. Y.; Choi, T. M.; Shim, T. S.; Frijns, R. A.; Kim, S. H. Microfluidic production of multiple emulsions and functional microcapsules. *Lab Chip* **2016**, *16* (18), 3415−3440.

(20) Jin, Z.; Wang, Y.; Liu, J.; Yang, Z. Synthesis and properties of paraffin capsules as phase change materials. *Polymer* **2008**, *49* (12), 2903−2910.

(21) Lee, T.; Trivedi, R. P.; Smalyukh, I. I. Multimodal nonlinear optical polarizing microscopy of long-range molecular order in liquid crystals. *Opt. Lett.* **2010**, *35* (20), 3447−3449.

(22) Trivedi, R. P.; Klevets, I. I.; Senyuk, B.; Lee, T.; Smalyukh, I. I. Reconfigurable interactions and three-dimensional patterning of colloidal particles and defects in lamellar soft media. *Proc. Natl. Acad. Sci. U. S. A.* **2012**, *109* (13), 4744−4749.

(23) Grigoriadis, C.; Duran, H.; Steinhart, M.; Kappl, M.; Butt, H.-J.; Floudas, G. Suppression of phase transitions in a confined rodlike liquid crystal. *ACS Nano* **2011**, *5* (11), 9208−9215.

(24) Kityk, A. V.; Wolff, M.; Knorr, K.; Morineau, D.; Lefort, R.; Huber, P. Continuous paranematic-to-nematic ordering transitions of liquid crystals in tubular silica nanochannels. *Phys. Rev. Lett.* **2008**, *101* (18), 187801.

(25) Peng, H. Y.; Shi, X. J.; Liao, Y. G.; Chen, D. T.; Wang, S. P.; Xie, X. L. Effects of different alcohols on photopolymerization kinetics, electro-optical performance of polymer dispersed liquid crystals. *Acta Polym. Sin.* **2012**, *012* (1), 41−46.

(26) Cavallo, G.; Metrangolo, P.; Milani, R.; Pilati, T.; Priimagi, A.; Resnati, G.; Terraneo, G. The halogen bond. *Chem. Rev.* **2016**, *116* (4), 2478−2601.

(27) Wang, C.; Danovich, D.; Mo, Y.; Shaik, S. On the nature of the halogen bond. *J. Chem. Theory Comput.* **2014**, *10* (9), 3726−3737.

(28) Ackerman, P. J.; Smalyukh, I. I. Diversity of knot solitons in liquid crystals manifested by linking of preimages in torons and hopfions. *Phys. Rev. X* **2017**, *7* (1), 011006.

(29) Ackerman, P. J.; Smalyukh, I. I. Reversal of helicoidal twist handedness near point defects of confined chiral liquid crystals. *Phys. Rev. E: Stat. Phys., Plasmas, Fluids, Relat. Interdiscip. Top.* **2016**, *93* (5), 052702.

(30) Trivedi, R. P.; Lee, T.; Bertness, K. A.; Smalyukh, I. I. Three dimensional optical manipulation and structural imaging of soft materials by use of laser tweezers and multimodal nonlinear microscopy. *Opt. Express* **2010**, *18* (26), 27658−27669.

(31) Peng, H. Y.; Yu, L.; Chen, G. N.; Bohl, T. W.; Ye, Y. S.; Zhou, X. P.; Xue, Z. G.; Roy, V. A. L.; Xie, X. L. Low-voltage-driven and highly-diffractive holographic polymer dispersed liquid crystals with spherical morphology. *RSC Adv.* **2017**, *7* (82), 51847−51857.

(32) Iannacchione, G. S.; Finotello, D. Calorimetric study of phase transitions in confined liquid crystals. *Phys. Rev. Lett.* **1992**, *69* (14), 2094−2097.